Heat capacity and structural transition effect in polycrystalline kesterite

Cédric Bourgès[1,*], Andrei Novitskii[2], Makoto Tachibana[2], Naoki Sato[2], and Takao Mori[2,3]

[1] *International Center for Young Scientists (ICYS), National Institute for Materials Science (NIMS), Namiki 1-1, Tsukuba, Ibaraki 305-0044, Japan*
[2]*MANA, National Institute for Materials Science (NIMS), Namiki 1-1, Tsukuba, Ibaraki 305-0044, Japan*
[3]*Graduate School of Pure and Applied Sciences, University of Tsukuba, Tennoudai 1-1-1, Tsukuba, Ibaraki 305-8577, Japan*

Corresponding Author: BOURGES.Cedric@nims.go.jp

Keywords: Kesterite, Heat Capacity, Cu_2ZnSnS_4,

Abstract:

As a crucial parameter in the determination of thermal conductivity, the heat capacity of $Cu_{2+x}Zn_{1-x}SnS_4$ (CZTS) has been investigated and analyzed in detail from 2 to 773 K. The effects of the Cu-Zn stoichiometric ratio and phase transition have been quantified and correlated with entropy variation. We confirm that the compounds follow the Dulong-Petit approximation above the Debye temperature θ_D and solve literature discrepancies on CZTS. The in-depth low-temperature heat capacity analysis revealed an approximate image of the energy dependance of the phonon density of state in kesterite which agrees with results of first-principles calculations.

The quaternary kesterite-Cu_2ZnSnS_4 (CZTS) is a well-reported *p*-type semiconductor with a wide bandgap ($E_g \approx$ 1.5 eV) attractive for light-absorber application in solar cells.[1] Recently, CZTS has also been investigated for thermoelectric (TE) applications due to the possibility of exploiting its phase transition at high temperatures together with Cu/Zn ratio modulation in order to promote a relatively high power factor ($PF = S^2\sigma$, with S, representing the Seebeck coefficient, and σ, representing the electrical conductivity) and low thermal conductivity (κ).[2–6] These two components compose the figure of merit of the thermoelectric materials zT ($= S^2\sigma T/\kappa$). In the TE field, the most common way to determine the thermal conductivity is an indirect method involving the independent measurements of thermal diffusivity D, heat capacity C_p, and density of the sample ρ, and using the formula, $\kappa = D \times C_p \times \rho$. The accuracy of these measurements is vital, as they collectively contribute to the reliable evaluation of a material's thermoelectric performance.

Recent reports on TE-CZTS highlighted promising zT values exceeding 1, which were obtained on both single-crystal[4] and polycrystalline samples.[3] However, these studies also indicated a significant discrepancy in the reported heat capacity of CZTS. For example, Nagaoka *et al.*[4,7] reported a high-quality ordered single crystal exhibiting a nearly monotonic heat capacity beyond its Debye temperature ($T \approx$ 307 K) aligned well with the Dulong-Petit approximation limit ($C_p = 3Nk_B = 0.459$ J.g^{-1}.K^{-1}), followed by a tiny drop in values above the phase transition of CZTS ($T \approx$ 500 K). In contrast, Jiang *et al.*[3] observed an anomalous peak in C_p near room temperature in polycrystalline samples, with heat capacity values varying from 0.23 to 0.44 J.g^{-1}.K^{-1} and a broad phase transition between 500 and 700 K.

The origin of these discrepancies and the role of the order-disorder structural transition and off-stoichiometry remain unclear and drive the necessity to set the accurate thermo-physical properties within the literature in order to construct a reliable material specification of the CZTS. Besides, the investigation of the low-temperature heat capacity can provide valuable insights into the role of the phonon vibrational mode and density of states in kesterite, extending the understanding of the thermal transport properties within this promising material.

For this purpose, the temperature dependence of the specific heat capacity of CZTS was investigated on polycrystalline samples from 2 to 773 K by combining the relaxation method measurement with Physical Properties Measurement System (PPMS), and the ratio method with differential scanning calorimetry (DSC). Those two methods present a high experimental accuracy within their respective range of temperature, of 1 – 5% for the PPMS ($T <$ 400 K) and 4 – 15% for the DSC method in a high-temperature range ($T >$ 350K).[8,9] For details on the measurement methodology, please refer to the supporting information (SI). Such comprehensive analysis aims to provide a clearer picture of the material's thermo-physical properties, paving the way for more accurate modeling and application of TE-CZTS in various technologies.

Two CZTS compositions have been prepared with nominal formula $Cu_{2+x}Zn_{1-x}SnS_4$, the native stoichiometry with x = 0 and the off-stoichiometry x = 0.125, which correspond to the optimum stoichiometry for TE application,[3,6] following the procedure described in the SI.

The crystal structure was investigated by high-temperature X-ray diffraction (HT-XRD) technique (Smart Lab 9kW Rigaku Corporation, Japan) with the prescriptive θ–2θ mode over a 10 – 120° angle range, a step size of 0.02° and a step time of 1.5°/min at each temperature, with thermalization of 5 min prior to the measurement which confirms the single-phase from 298 to 673 K during both the heating and cooling cycles (**Fig. 1**). The extra reflection (▼) being attributed to the Al_2O_3 HT-XRD holder. To confirm this, a Rietveld refinement have been performed on the routine room temperature scan with the Al_2O_3 holder which confirmed the ordered structure of the kesterite through low reliability factor (**S1-S2**).

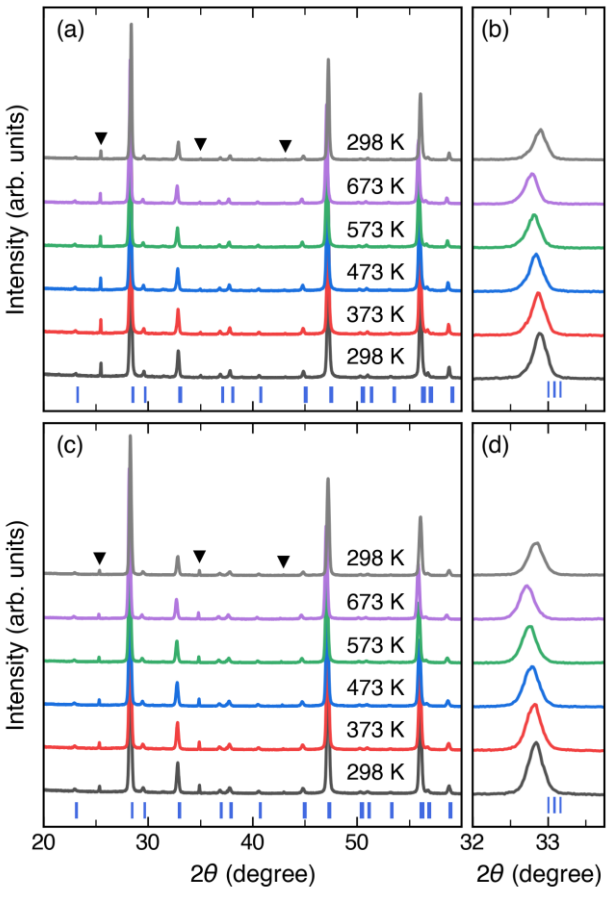

Figure 1. High-temperature X-ray diffraction patterns of $Cu_{2+x}Zn_{1-x}SnS_4$ with (a) x = 0 and (c) x = 0.125 during heating from 298 to 673 K and at room temperature after cooling. (b, d) Enlarged sections for the corresponding samples in a 2θ range from 32° to 34°. Peaks corresponding to the Al_2O_3 HT-XRD sample holder are indicated by black solid triangles (▼).

Figures 1b and d highlight a characteristic indexation at 2θ = 32.9°, which can be representative of the order-disorder transition as subject to a noticeable shape change between the two similar structures. However, it can be observed that no definitive conclusion can be extracted from HT-XRD despite the standard resolution of the apparatus employed even on the lattice parameters trend obtained through pattern matching refinement of the pattern (**Fig. S3**). This illustrates that the phase transition, usually occurring around $T \approx 500 - 550$ K, from ordered to disordered structure cannot be captured by conventional XRD crystal structure characterization.

The temperature-dependent heat capacity C_p, studied from 315 to 773 K, was determined by Differential Scanning Calorimetry (DSC 404 Netzsch, Germany) measurement system using the ratio method and a sapphire standard reference in Al crucibles. The slightly lower accuracy reported for the DSC compared to the PPMS comes usually from the lack of isothermal holding and/or sample–reference mass mismatch. To mitigate this, a specific care was taken during the measurement of two bulk samples for each composition with different mass and an isothermal hold of 50 min before the dynamic segment.[9] For the low temperature range from 2 to 305 K, C_p measurements were performed using a Quantum Design physical property measurement system (PPMS) employing a relaxation method. Apiezon N high vacuum grease was applied to provide sufficient thermal contact between the sample and the platform in the high-vacuum environment during the measurement (see in SI for details).

Figure 2 displays the C_p of polycrystalline CZTS (x = 0, 0.125) from 2 to 773 K and compared it with the literature data available on single-crystal and polycrystalline CZTS and rationalized by a theoretical estimation from phonon analysis based on our Density Functional Theory (DFT) calculation (see in SI for details). It reveals that beyond θ_D ($\approx$ 300 K)[7] the C_p behaves like a typical transition metal sulfide with values reaching the Dulong-Petit limit of $3Nk_B$ (C_p = 0.459 J.g^{-1}.K^{-1}) in the continuity of the accurate PPMS measurements, and thus, independently to the sample off-stoichiometry. These values are consistent with the data obtained on high-quality single-crystal by Nagaoka *et al.*[4,7] However, it is in conflict with reports on polycrystalline samples by Isotta *et al.* and Jiang *et al.*[3,10], wherein the C_p trends and values are drastically divergent (**Fig. 2- yellow hexagon and red stars**). Apart from the fact that the Isotta's report shows values out of the thermo-physical range of any transition metal sulfides, the results of the Jiang's report approach the Dulong-Petit limit around $T \approx 400 - 500$ K before significantly decreasing to values two times lower than that for the single-crystal and our data in the high-temperature range. The authors explained this behavior by a possible liquid-like state of the Cu-Zn sites which is unevidenced. Moreover, in a case of liquid like behavior, phase transition would likely increase the CZTS-C_p because of the higher degrees of freedom and therefore greater entropy acquired by the Cu-Zn. In our samples, for each composition, a peak attributed to the structural transition is observed at $T \approx$ 558 K and 507 K for x = 0 and 0.0125 (**Fig. S4**), respectively. It corresponds to the structural transition from ordered to disordered CZTS where Cu-2*c* site and Zn-2*d* site in ($I\bar{4}$) lattice mixed their occupancy and form the Cu/Zn-4*d* site in the ($I\bar{4}2m$) lattice. Due to the very similar crystal structure, the transition is undetectable by conventional structural characterization like HT-XRD (**Fig. 1**) but clearly visible through the C_p temperature dependence. The transition occurred also on the ordered single crystal ($T \approx$ 550 K) but was not observed on the disordered one (**Blued triangle in Fig. 2**). Interestingly, we revealed that the native stoichiometry affects the phase transition temperature and $Cu_{2.125}Zn_{0.875}SnS_4$ exhibited a lower transition temperature. However, no significant changes in C_p are observed after the transition which at the end tends to merge with the theoretical Dulong-Petit limit.

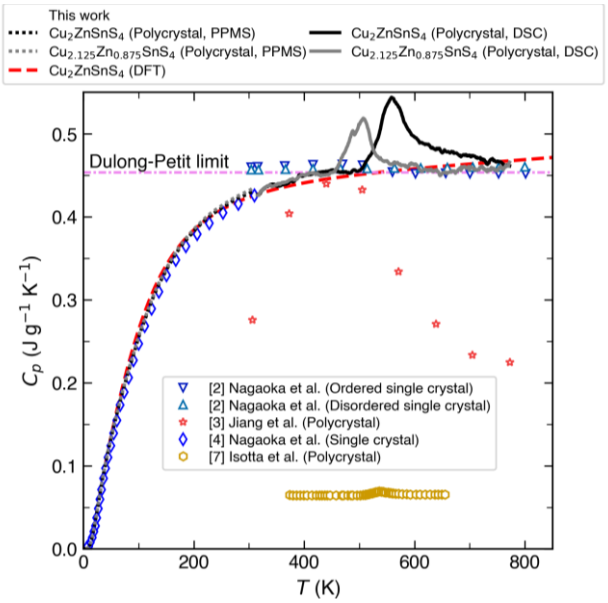

Figure 2. The heat capacity C_p comparison as a function of temperature from 2 to 773 K of current work $Cu_{2+x}Zn_{1-x}SnS_4$ (x = 0, 0.125) with state of the art of polycrystal[3,10] and single crystal samples[4,7] of CZTS kesterite. The red dashed line corresponds to the theoretical C_p values determined by DFT calculations.

The lower transition temperature of the x = 0.125 sample agrees with the destabilized ordered state induced by the Cu/Zn off-stoichiometry. This is confirmed and illustrated by the reduction of the entropy variation at the phase transition from ΔS = 8.72 mJ.g^{-1}K^{-1} to ΔS = 6.93 mJ.g^{-1}K^{-1} for x = 0 and 0.125, respectively. The entropy variation can be estimated by integration of the phase transition peak of C_p following this equation (**Fig. S4**):

$$\Delta S = \int \frac{Cp}{T} dT$$

Besides the obvious difference in the heat capacity values discussed in the previous section, it is also important to consider the low-temperature range of heat capacity, which can provide insights into disorder and various contributions of phonon modes to the total heat capacity. The temperature dependence of the C_p, normalized by the molar mass, for $Cu_{2+x}Zn_{1-x}SnS_4$ (x = 0, 0.125) is depicted in **Figure 3**, covering the temperature range from 2 to 300 K. The heat capacity for both compositions, Cu_2ZnSnS_4 and $Cu_{2.125}Zn_{0.875}SnS_4$, is almost the same, reaching a value of 190 J mol^{-1} K^{-1} at room temperature, which is close to the classical high-temperature limit.

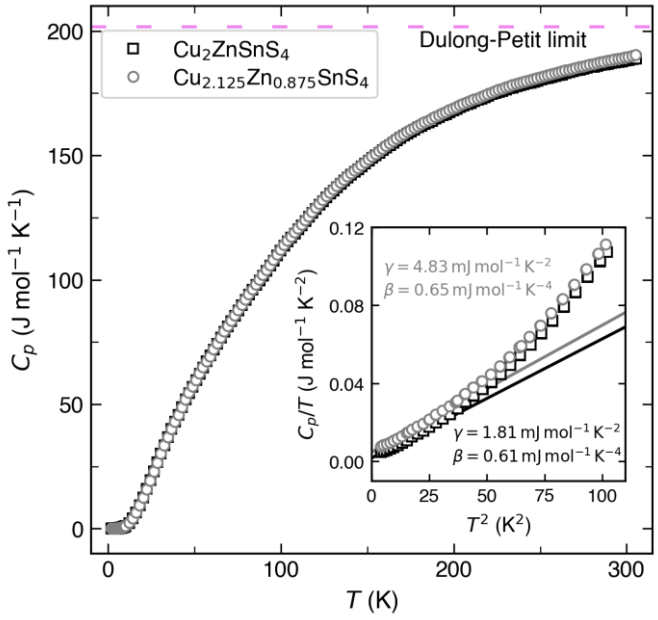

Figure 3. The heat capacity C_p of $Cu_{2+x}Zn_{1-x}SnS_4$ (x = 0, 0.125) as a function of temperature from 2 to 300 K. The inset shows the low-T C_p data plotted as C_p/T versus T^2.

The inset in **Fig. 3** shows the C_p data below 10 K plotted on a C_p/T versus T^2 scale allowing a conventional fit by

$$C_p(T) = \beta T^3 + \gamma T$$

where β represents the Debye T^3 lattice heat capacity coefficient at low temperatures, and the linear term γ is related to disorder as the contribution from conduction electrons is negligible in this large bandgap semiconductor ($E_g \approx 1.5$ eV).[11,12] C_p values of both samples can be fitted within a limited temperature range and β values obtained from the linear fit display only minor fluctuations among the two samples (**Table 1**). Thus, the Debye temperature θ_D calculated from β as

$$\theta_D = \left(\frac{12\pi^4 N_A k_B n}{5\beta}\right)^{1/3}$$

with N_A representing Avogadro's number, k_B is Boltzmann's constant, and n is the number of atoms per formula unit, is around 290 K (**Table 1**), which is consistent with previously reported data for Cu_2ZnSnS_4 single crystal,[7] suggesting that deviations from stoichiometry have a minor influence on θ_D. In contrast, γ increases from 1.81 mJ mol^{-1} K^{-2} to 4.83 mJ mol^{-1} K^{-2} as off-stoichiometry is introduced.

This is consistent with the Cu-Zn mixed occupancy at the Zn (2*d*) site, which creates a "virtual" disorder similar to the phase transition above T > 500 K with a common 4*d* site for Cu-Zn in a $I\bar{4}2m$ space group lattice. Therefore, it shows that low-T C_p measurements can provide experimental evidence of the degree of disorder in CZTS. This insight is highly valuable as it has been evidence that the disorder state in kesterite affects its electronic density of state $g(E_F)$ by increasing the steepness at the top of the valence band near the Fermi energy.[10,13] According to the Mott's formula,[14] the modification of the electronic DOS is consistent with the larger Seebeck coefficient promoted by the disorder state in CZTS making it beneficial for TE properties as it enhances the *PF* of the material.

Table 1. The coefficient γ, the coefficient of the Debye T^3 lattice heat capacity β, and the Debye temperature θ_D from low temperature heat capacity measurements for $Cu_{2+x}Zn_{1-x}SnS_4$ (x = 0, 0.125).

Sample	γ (mJ mol^{-1} K^{-2})	β (mJ mol^{-1} K^{-4})	θ_D (K)
Cu_2ZnSnS_4	1.81	0.612	294
$Cu_{2.125}Zn_{0.875}SnS_4$	4.83	0.651	288

The Debye theory of lattice heat capacity presumes a linear dispersion for acoustic lattice vibrations. The observed deviation suggests the presence of excitations beyond a simple Debye contribution arising from acoustic modes (**inset in Fig. 3**). These contributions are even more evident when the data are plotted as C_p/T^3 versus ln$T$, as shown in **Fig. 4**. This plot is particularly insightful for identifying the various contributions of vibrational modes to heat capacity since it can be considered as an approximate representation of $D(\omega)/\omega^2$ versus $\ln(\hbar\omega/4.93k_BT)$, with $D(\omega)$ denoting the phonon spectrum.[15] For $Cu_{2+x}Zn_{1-x}SnS_4$ (x = 0, 0.125) samples, one additional feature revealed in this plot is the broad peak around ln$T \approx 3$ ($T \approx 20$ K) indicating the presence of optical vibrational modes. The most noticeable difference between the two samples is the sharply increasing low-temperature

tail (ln$T$ < 2), which corresponds to the linear component (**Fig. S5**).

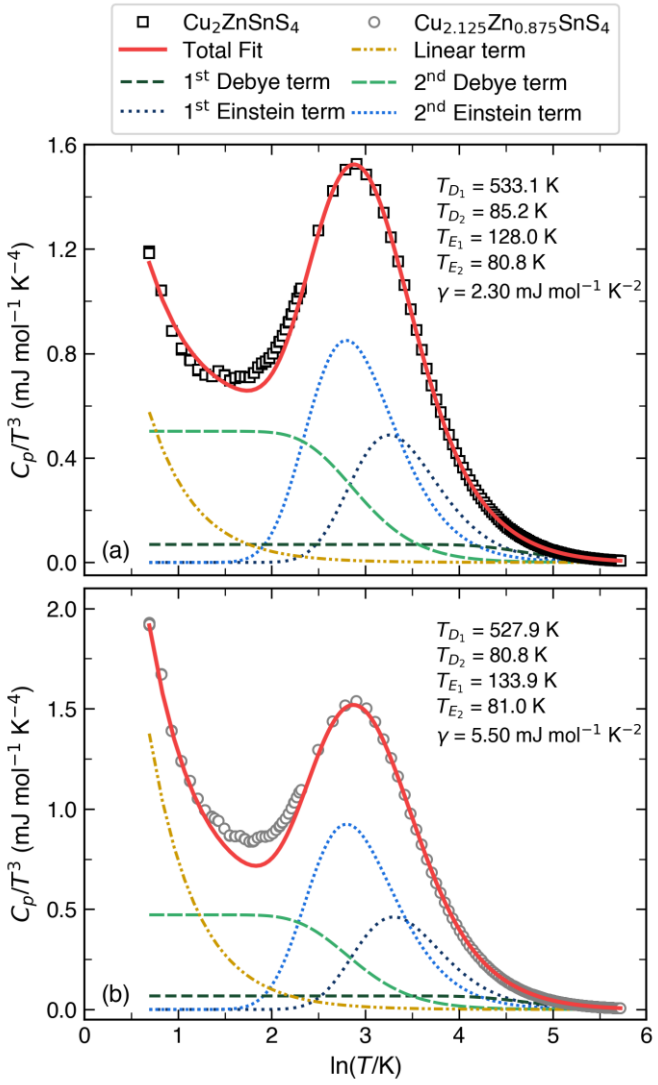

Figure 4. The heat capacity C_p of (a) Cu_2ZnSnS_4 and (b) $Cu_{2.125}Zn_{0.875}SnS_4$ plotted as C_p/T^3 versus ln$T$. Experimental data presented as gray and black empty symbols, while green dashed, blue dotted, and yellow dashed lines represent Debye, Einstein, and linear contributions. Solid red line represents total fit.

To quantify the modes contributing to the measured heat capacity, we used a conventional approach that involves the fitting of the experimental data with a model containing Debye, Einstein, and linear components. For the acoustic modes, the Debye term (**dashed lines in Fig. 4**):

$$C_{p,D}(T) = 9nR\left(\frac{T}{\theta_D}\right)^3 \int_0^{\theta_D/T} \frac{x^4 e^x}{(e^x-1)^2}\,dx$$

was used with the only two variables: the effective Debye temperature θ_D and the oscillator strength per formula unit (f.u.). To model the optical modes responsible for the peak around 20 K, an Einstein term (**dotted lines in Fig. 4**)

$$C_{p,E}(T) = 3nR\left(\frac{\theta_E}{T}\right)^2 \frac{e^{\theta_E/T}}{(e^{\theta_E/T}-1)^2}$$

was necessary. Finally, a significant linear component $C_{p,S}(T) = \gamma T$ had to be considered (**dotted dashed line in Fig. 4**). The best fit to the measured data was obtained with the five contributions characterized by a total of nine parameters (see **Table 2**). Each separate contribution along with total fit and the experimental data are plotted in **Fig. 4**. The energy and oscillator strength of the Debye and Einstein terms obtained from the fit are listed in **Table 2**.

The two Einstein modes used for the fit represent two optical phonon mode frequencies at 152 cm^{-1} and 232 cm^{-1} for x = 0 and agree with the calculated PDOS (**Fig. S6**).[16,17] The phonon mode at 152 cm^{-1} corresponds to the major contribution of the cations (Cu-Zn-Sn), while the mode at 232 cm^{-1} can be attributed mostly to the Cu and S contributions.[16] Spectral weight of the Einstein mode, in turn, is about 2.6-2.8 oscillators/f.u. corresponding to around 1/3 of the total number of degrees of freedom in the solid. The phonon mode frequencies and oscillator strength do not vary significantly with the off-stoichiometry x = 0.125 (**Table 2**), suggesting that the Zn_{Cu} antisite defect plays a minor role in the phonon vibrational modes.

Table 2. Einstein modes frequencies, effective Debye modes temperature, and Sommerfield constant for $Cu_{2+x}Zn_{1-x}SnS_4$ (x = 0, 0.125).

Sample	Cu_2ZnSnS_4	
Mode	Energy	Oscillator Strengh /f.u.
E_1 (cm^{-1})	151.7	1.816
E_2 (cm^{-1})	232.0	0.790
θ_{D1} (K)	85.2	5.234
θ_{D2} (K)	533.1	0.160
γ (mJ mol^{-1} K^{-2})	2.3	–
Sample	$Cu_{2.125}Zn_{0.875}SnS_4$	
Mode	Energy	Oscillator Strengh /fu.u.
E_1 (cm^{-1})	160.2	1.990
E_2 (cm^{-1})	260.5	0.837
θ_{D1} (K)	81.0 K	5.054
θ_{D2} (K)	527.9 K	0.120
γ (mJ mol^{-1} K^{-2})	5.5	–

The solely linear term provides a reasonable fit in the T dependence of C_p (**Fig. 2 and S7**) but it is worth noting that the low-T fit (below ln$T$ < 2) is not fully matching with the

experimental data (**Fig. 4**). An additional fit (**Fig. S8**), including a Schottky term, was performed to provide a fair improvement of the low-*T* fit. The Schottky anomalies can be attributed to the presence of lattice vacancies which induce a linear temperature dependence of C_p, similar to that of conduction electrons, in a non-metals sample and can be described using the following equation:[12]

$$C_{p,Sch}(T) = n_{Sch} R \left(\frac{\Delta}{T}\right)^2 \frac{e^{\Delta/T}}{(1+e^{\Delta/T})^3}$$

where Δ is the energy separation of the two states in Kelvin, n_{Sch} is the moles of anomalies per formula unit for a given separation Δ, and R representing the molar gas constant. As a results, the energy and contributions of the Debye and Einstein modes remain mostly unchanged (**Fig. S8**), supporting the accuracy of the prior conclusions regarding the phonon mode contributions. However, the Schottky contribution appears larger in the x = 0.125 sample, suggesting the possibility of a larger number of lattice vacancies in the sample.[12]

We thoroughly investigated the heat capacity of CZTS on stoichiometric and off-stoichiometric polycrystalline samples in a broad temperature range (T = 2 – 773 K) to understand the discrepancies in the reported thermal conductivity of this promising ceramic for thermoelectric applications. We confirmed and determined accurate C_p values on bulk samples comparable to single crystals and show that the CZTS behaves like a typical transition metal sulfide reaching the Dulong-Petit limit at high temperatures following the classical statistical Boltzmann theory with the full vibrational mode restrict to 3 degrees of freedom in the solid, i.e., no additional degree of freedom from liquid-like state of Cu-Zn. We highlighted that the structural transition temperature from ordered to disordered CZTS is affected by the Cu-Zn off-stoichiometry consistently with a reduction of the entropy variation in the off-stoichiometric CZTS. We determined the Debye temperature, the contribution of disorder, and the Einstein modes through low-temperature heat capacity measurements, which showed a good agreement with reported phonon density of states calculations. Our study evidences that C_p studies are not only crucial to obtain consistent and accurate thermal transport properties but also useful in the understanding of the transport properties as it enable the possibility to quantify partially the order-disorder phase transition as well as the "native disorder" induced by off-stoichiometry directly related to the electronic band structure of this material.

Conflicts of interest

There are no conflicts to declare.

Acknowledgements

This work was supported by International Center for Young Scientist (ICYS) Fellowship (NIMS, Japan), and JST Mirai Program JPMJMI19A1. The authors would like to acknowledge Material Analysis Station (NIMS, Japan) for the XRD analysis.

References:

1 A. Wang, M. He, M. A. Green, K. Sun and X. Hao, *Adv. Energy Mater.*, 2023, **13**, 2203046.

2 E. Isotta, N. M. Pugno and P. Scardi, *Powder Diffr.*, 2019, **34**, S42–S47.

3 Q. Jiang, H. Yan, Y. Lin, Y. Shen, J. Yang and M. J. Reece, *J. Mater. Chem. A*, 2020, **8**, 10909–10916.

4 A. Nagaoka, K. Yoshino, T. Masuda, T. D. Sparks, M. A. Scarpulla and K. Nishioka, *J. Mater. Chem. A*, 2021, **9**, 15595–15604.

5 A. Nagaoka, S. Miura, K. Nakashima, Y. Hirai, T. Higashi, K. Yoshino and K. Nishioka, *Appl. Phys. Lett.*, 2024, **125**, 072101.

6 C. Bourgès, G. Lambard, N. Sato, M. Tachibana, S. Ishii and T. Mori, *Acta Mater.*, 2024, **281**, 120342.

7 A. Nagaoka, K. Yoshino, K. Aoyagi, T. Minemoto, Y. Nose, T. Taniyama, K. Kakimoto and H. Miyake, *J. Cryst. Growth*, 2014, **393**, 167–170.

8 C. A. Kennedy, M. Stancescu, R. A. Marriott and M. A. White, *Cryogenics*, 2007, **47**, 107–112.

9 H. Wang, W. D. Porter, H. Böttner, J. König, L. Chen, S. Bai, T. M. Tritt, A. Mayolet, J. Senawiratne, C. Smith, F. Harris, P. Gilbert, J. Sharp, J. Lo, H. Kleinke and L. Kiss, *J. Electron. Mater.*, 2013, **42**, 1073–1084.

10 E. Isotta, C. Fanciulli, N. M. Pugno and P. Scardi, *Nanomaterials*, 2019, **9**, 762–773.

11 P. w. Anderson, B. I. Halperin and c. M. Varma, *Philosophical Magazine*, 1972, **25**, 1–9.

12 J. M. Schliesser and B. F. Woodfield, *Phys. Rev. B*, 2015, **91**, 024109.

13 E. Isotta, B. Mukherjee, C. Fanciulli, N. M. Pugno and P. Scardi, *Journal of Phys. Chem. C*, 2020, **124**, 7091–7096.

14 F. A. Rohrman, *J. Chem. Educ.*, 1937, **14**, 99.

15 A. Junod, T. Jarlborg and J. Muller, *Phys. Rev. B*, 1983, **27**, 1568–1585.

16 A. Khare, B. Himmetoglu, M. Johnson, D. J. Norris, M. Cococcioni and E. S. Aydil, *J. Appl. Phys.*, 2012, **111**, 083707.

17 A. J. Jackson and A. Walsh, *J. Mater. Chem. A*, 2014, **2**, 7829–7836.